Inorganic Chemistry

Article

pubs.acs.org/IC

Bis(cyano) Iron(III) Porphyrinates: What Is the Ground State?

Jianfeng Li,*[,†] Bruce C. Noll,[‡] Charles E. Schulz,*[,§] and W. Robert Scheidt*[,‡]

[†]College of Materials Science and Optoelectronic Technology, University of Chinese Academy of Sciences, YanQi Lake, HuaiRou District, Beijing 101408, China

[‡]Department of Chemistry and Biochemistry, University of Notre Dame, Notre Dame, Indiana 46556, United States

[§]Department of Physics, Knox College, Galesburg, Illinois 61401, United States

Supporting Information

ABSTRACT: The synthesis of six new bis(cyano) iron(III) porphyrinate derivatives is reported. The anionic porphyrin complexes utilized tetraphenylporphyrin, tetramesitylporphyrin, and tetratolylporphyrin as the porphyrin ligand. The potassium salts of Kryptofix-222 and 18-C-6 were used as the cations. These complexes have been characterized by X-ray structure analysis, solid-state Mössbauer spectroscopy, and EPR spectroscopy, both in frozen CH_2Cl_2 solution and in the microcrystalline state. These data show that these anionic complexes can exist in either the $(d_{xz},d_{yz})^4(d_{xy})^1$ or the $(d_{xy})^2(d_{xz},d_{yz})^3$ electronic configuration and some can clearly readily interconvert. This is a reflection that these two states can be very close in energy. In addition to the effects of varying the porphyrin ligand, subtle effects of the cyanide ligand environment in the solid state and in solution are sufficient to shift the balance between the two electronic states.

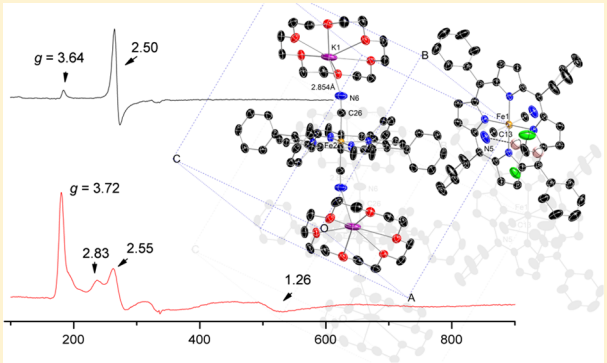

INTRODUCTION

Cyanide ion, CN^-, a well-known acute chemical poison, acts by inhibiting the enzyme cytochrome *c* oxidase, which catalyzes the conversion of O_2 to H_2O along with captured biological energy necessary to sustain life.[1−3] The cyanide ion readily yields low-spin (cyano)iron(III) derivatives when there is a vacant coordination site at the heme in hemoproteins[4] and is frequently used as an inhibitor to study hemoproteins such as oxidases and peroxidases.[5] Peroxidases such as horseradish peroxidase, lactoperoxidase, and chloroperoxidase use cyanide as an inhibitory substrate and catalyze the one-electron oxidation to form the cyanyl radical.[6,7]

Moreover, the cyanide ligand is an important ligand in its own right. Although it is widely regarded as a strong field ligand in coordination chemistry, the reality is more complex with a number of electronic and geometric structure issues. We have characterized two different polymorphic forms of a five-coordinate iron(II) species, [K(222)][Fe(TPP)(CN)]. Although both forms are low-spin species at low temperatures, both undergo a gradual spin-state transition to the high-spin state that is still not quite complete at 400 K.[8,9] Structural parameters as well as physical properties (Mössbauer, magnetic susceptibility, and IR) display appropriate changes in values for this $S = 0 \leftrightharpoons S = 2$ spin equilibrium. Thus, the coordination of cyanide is more complex than that of simply a strong field ligand. However, the iron(II) bis(cyanide) porphyrinates are pure low-spin species.

The iron(III) bis(cyanide) porphyrinates are also low-spin species. Reports by Nakamoto and co-workers[10−15] showed that many bis(cyano) iron(III) porphyrinates displayed (in varying solvents) axial EPR spectra consistent with the unusual $(d_{xz},d_{yz})^4(d_{xy})^1$ ground state, whereas others could be induced to display the more usual $(d_{xy})^2(d_{xz},d_{yz})^3$ electronic state. We had previously shown that one single iron(III) bis(cyanide) iron(III) porphyrinate could display the two different electronic structures in the solid and solution states,[16] yet both are low-spin species. Clearly, further study of bis(cyano) heme derivatives could hold additional unexpected results.

In this Article, we have further explored the issue of the electronic structure of the bis(cyano) iron(III) porphyrinates. We report the synthesis, X-ray, and physical characterization of six new bis(cyano) iron(III) porphyrinates. We find that the data for these derivatives (e.g., the Mössbauer and EPR spectra) are consistent with the formation of two electronic states defined by the orbital populations $(d_{xz},d_{yz})^4(d_{xy})^1$ or $(d_{xy})^2(d_{xz},d_{yz})^3$. Importantly, the two states must be, at least in some cases, very close in energy, and the small structural differences can tip the balance between the two states. Significantly, we are unable to identify a single feature of this group of bis(cyanide) derivatives that defines which electron state will be observed.

EXPERIMENTAL SECTION

General Information. THF was distilled over sodium and benzophenone ketyl; all other solvents were used as received (Fisher).

Received: April 7, 2015
Published: June 22, 2015

DOI: 10.1021/acs.inorgchem.5b00780
Inorg. Chem. 2015, 54, 6472−6485

Table 1. Complete Crystallographic Details for $[K(18\text{-}C\text{-}6)][Fe(TPP)(CN)_2]\cdot 3CH_2Cl_2$, $[K(18\text{-}C\text{-}6)][Fe(TPP)(CN)_2]\cdot 3.5CH_2Cl_2$, $[K(222)][Fe(TPP)(CN)_2]\cdot 3.5CH_2Cl_2$, $[K(222)][^{57}Fe(TPP)(CN)_2]$, $[K(222)][^{57}Fe(TMP)(CN)_2]\cdot 3CH_2Cl_2$, and $[K(222)][^{57}Fe(TTP)(CN)_2]\cdot 2CH_2Cl_2$

	$[K(18\text{-}C\text{-}6)][Fe(TPP)(CN)_2]\cdot 3CH_2Cl_2$	$[K(18\text{-}C\text{-}6)][Fe(TPP)(CN)_2]\cdot 3.5CH_2Cl_2$	$[K(222)][Fe(TPP)(CN)_2]\cdot 3.5CH_2Cl_2$	$[K(222)][^{57}Fe(TPP)(CN)_2]$	$[K(222)][^{57}Fe(TMP)(CN)_2]\cdot 3CH_2Cl_2$	$[K(222)][^{57}Fe(TTP)(CN)_2]\cdot 2CH_2Cl_2$
chemical formula	$C_{61}H_{57}Cl_6FeKN_6O_6$	$C_{61.5}H_{59}Cl_7FeKN_6O_6$	$C_{67.50}H_{71}Cl_7FeKN_8O_6$	$C_{64}H_{64}FeKN_8O_6$	$C_{79}H_{94}Cl_6FeKN_8O_6$	$C_{70}H_{76}Cl_4FeKN_8O_6$
FW	1277.78	1321.25	1433.42	1136.18	1559.28	1362.14
a, Å	12.9810(6)	12.8299(1)	14.0118(7)	20.6780(7)	11.4858(3)	31.8765(12)
b, Å	19.2098(9)	15.6896(2)	14.3881(7)	13.5854(5)	14.0967(4)	16.4605(6)
c, Å	24.3751(12)	17.3858(2)	18.9426(9)	21.9944(11)	26.9709(7)	13.7573(5)
α, deg	90.00	70.3520(1)	69.834(2)	90.00	97.3010(1)	90.00
β, deg	99.583(2)	75.0480(1)	73.549(2)	112.213(1)	90.7850(1)	105.612(2)
γ, deg	90.00	70.7100(1)	80.577(2)	90.00	113.8940(1)	90.00
V, Å^3	5993.4(5)	3068.10(6)	3428.8(3)	5720.1(4)	3950.03(18)	6952.2(4)
space group	$P2_1/c$	$P\bar{1}$	$P\bar{1}$	$C2/c$	$P\bar{1}$	$C2/c$
Z	4	2	2	4	2	4
temp, K	100	100	100	100	100	100
D_{calcd}, g cm^{-3}	1.416	1.430	1.388	1.319	1.311	1.301
μ, mm^{-1}	0.645	0.674	0.610	0.396	0.503	0.487
final R indices $[I > 2\sigma(I)]$	$R_1 = 0.0641$ $wR_2 = 0.1531$	$R_1 = 0.0620$ $wR_2 = 0.1498$	$R_1 = 0.0483$ $wR_2 = 0.1229$	$R_1 = 0.0381$ $wR_2 = 0.0947$	$R_1 = 0.0433$ $wR_2 = 0.1045$	$R_1 = 0.0588$ $wR_2 = 0.1545$
final R indices	$R_1 = 0.0953$	$R_1 = 0.0804$	$R_1 = 0.0670$	$R_1 = 0.0471$	$R_1 = 0.0536$	$R_1 = 0.0904$
s (all data)	$wR_2 = 0.1776$	$wR_2 = 0.1664$	$wR_2 = 0.1375$	$wR_2 = 0.1002$	$wR_2 = 0.1119$	$wR_2 = 0.1793$

1,4,7,10,13,16-Hexaoxacyclooctadecane (18-C-6) and Kryptofix 222 (222) (Aldrich)[17] were used as received. KCN was recrystallized and purified by a literature procedure.[18] *meso*-Tetraphenylporphyrin was prepared according to Adler et al.,[19] and *meso*-tetramesitylporphyrin by a modified version of the procedure published by Lindsey et al.[20] The metalation of the free-base porphyrins to give [Fe(Porph)Cl] was done as previously described.[21] 95% isotopically enriched [^{57}Fe(Porph)(Cl)] was prepared using the metalation procedure described by Landergren and Baltzer.[22] This was converted to [^{57}Fe(Porph)]$_2$O by shaking with KOH solution and drying over $MgSO_4$.[23] UV−vis spectra were recorded on a PerkinElmer Lambda 19 UV/vis/near-IR spectrometer, and IR spectra were recorded on a Nicolet Nexus 670 FT-IR spectrometer as KBr pellets. EPR spectra were recorded on powder samples obtained by grinding a sufficient quantity of the crystalline samples. Solution measurements were made by dissolving the samples in methylene chloride. EPR spectra were collected on a Bruker EMX EPR spectrometer. For measurements at 4−6 K, a cavity with attached Oxford continuous flow cryostat (ESR 900) was used. Spectra were collected and analyzed using Bruker's EPR Acquisition and WinEPR programs. Mössbauer measurements were performed on a constant acceleration spectrometer from 4.2 to 300 K with optional small field and in a 9 T superconducting magnet system (Knox College). Samples for Mössbauer spectroscopy were prepared by immobilization of the crystalline material in Apiezon M grease.

Synthesis of $[K(18\text{-}C\text{-}6)][Fe(TPP)(CN)_2]\cdot 3CH_2Cl_2$ (Needle Form) and $[K(18\text{-}C\text{-}6)][Fe(TPP)(CN)_2]\cdot 3.5CH_2Cl_2$ (Block Form). $[Fe(TPP)(H_2O)_2]ClO_4$ was prepared as described previously.[24] KCN (20 mg, 0.31 mmol) and 18-crown-6 (50 mg, 0.19 mmol) were added to a solution of $[Fe(TPP)(H_2O)_2]ClO_4$ (56 mg, 0.07 mmol) in toluene. The mixture was stirred overnight and dried to a black powder in a vacuum. Methylene chloride was then added, and the solution was stirred for an additional 5 h. The solution was divided into two 8 mm crystallizing tubes, and crystals were obtained by slow diffusion of hexanes into the reaction solution. In most tubes, two crystalline forms were observed, although occasionally only one phase was observed. The two crystalline forms were physically separated under a microscope. Microhomogeneity was assured by Mössbauer spectroscopy. The block form crystals are notably fragile. IR ν(C−N): (block form) 2115 cm^{-1}. IR (needle form) ν(C−N): 2114 cm^{-1}.

Synthesis of $[K(222)][Fe(TPP)(CN)_2]\cdot 3.5CH_2Cl_2$. KCN (20 mg, 0.31 mmol) and Kryptofix-222 (38 mg, 0.1 mmol) were added to a solution of $[Fe(TPP)(H_2O)_2]ClO_4$ (56 mg, 0.07 mmol) in CH_2Cl_2. The mixture was stirred overnight. Hexanes was then allowed to diffuse slowly into this reaction solution. Several days later, the block crystalline product was collected. IR ν(C−N): 2114 cm^{-1}.

Synthesis of $[K(222)][^{57}Fe(TPP)(CN)_2]$, $[K(222)][^{57}Fe(TMP)(CN)_2]\cdot 3CH_2Cl_2$, $[K(222)][^{57}Fe(TTP)(CN)_2]\cdot 2CH_2Cl_2$. These three complexes are accidental products in attempts to prepare the 5-coordinate $[K(222)][^{57}Fe(Porph)(CN)]$ complex.[8] In a typical reaction procedure, KCN (5.3 mg, 0.08 mmol) and Kryptofix-222 (31 mg, 0.08 mmol) were added to a CH_2Cl_2 solution of [^{57}Fe(Porph)] (50 mg, 0.08 mmol), which was obtained by reduction of [^{57}Fe(Porph)]$_2$O in benzene by ethanethiol (0.5 mL). The mixture was stirred overnight, and hexanes was allowed to diffuse in slowly. Unexpected oxidation happened and crystalline product was obtained. IR ν(C−N): 2113, 2113, and 2110 cm^{-1}, respectively.

X-ray Structure Determinations. Single-crystal experiments were carried out on Bruker Apex systems with graphite monochromated Mo K_α radiation (λ = 0.71073 Å). Crystals were placed in inert oil, mounted on a glass pin, and transferred to the cold gas stream of the diffractometer, and crystal data were collected at 100 K, except $[K(222)][^{57}Fe(TPP)(CN)_2]$, which was mounted in a sealed capillary and measured at 100 and 298 K. The structures were solved by direct methods (SHELXS-97)[25] and refined against F^2 using SHELXL-97.[26,27] Subsequent difference Fourier syntheses led to the location of all remaining nonhydrogen atoms. For the structure refinement, all data were used including negative intensities. All nonhydrogen atoms were refined anisotropically if not remarked upon otherwise below. Hydrogen atoms were idealized with the standard SHELXL-97 idealization methods. The program SADABS[28] was applied for the absorption correction. Complete crystallographic details, atomic coordinates, anisotropic thermal parameters, and fixed hydrogen atom coordinates are given in the Supporting Information tables for all six structures; a brief description of crystallographic details is given in Table 1.

Solid-state analysis of crystal packing distances made use of the program MERCURY[29] from the Cambridge Crystallographic Data Center. Environmental effects in the form of intermolecular nonbonded contacts close to the cyanide nitrogen atom position were examined with the program MERCURY (values of the van der Waals radii were taken from ref 30). It should be noted that all values involving the hydrogen atom of the CH_2Cl_2 solvent are based on an idealized position of this hydrogen atom.

DOI: 10.1021/acs.inorgchem.5b00780
Inorg. Chem. 2015, 54, 6472−6485

[K(18-C-6)][Fe(TPP)(CN)$_2$]·3.5CH$_2$Cl$_2$ (Block Form). A dark purple crystal with the dimensions 0.42 × 0.35 × 0.27 mm was used for the structure determination. The asymmetric unit contains two independent half-[Fe(TPP)(CN)$_2$]$^-$ anions, each with required inversion symmetry, one disordered 18-crown-6, and three and one-half methylene chloride solvent molecules. The crown ether unit was refined as two orientations of the entire 18-crown-6 ring with a single K$^+$ position. The first methylene chloride is ordered. The second and third methylene chloride are refined as three orientations of the entire molecule with the occupancies restrained to one and the C−Cl distances constrained by means of DFIX commands. The final half-molecule of methylene chloride was disordered around an inversion center with two chlorine positions and the carbon related by the center.

[K(18-C-6)][Fe(TPP)(CN)$_2$]·3CH$_2$Cl$_2$ (Needle Form). A black crystal with the dimensions 0.25 × 0.19 × 0.16 mm was used for the structure determination. The asymmetric unit contains one porphyrin complex, one ordered 18-crown-6 ether, and three methylene chloride solvent molecules. One of the methylene chlorides was disordered, and both chlorine atoms were refined over two positions.

[K(222)][Fe(TPP)(CN)$_2$]·3.5CH$_2$Cl$_2$. A dark purple crystal with the dimensions 0.29 × 0.21 × 0.17 mm was used for the structure determination. The asymmetric unit contains one porphyrin complex and one ordered Kryptofix-222 molecule. There are three and one-half disordered methylene chloride solvent molecules. The three whole methylene chlorides were refined as several positions, and the occupancies for each molecule are restrained to one; the C−Cl distances are constrained by means of DFIX commands. For the one-half methylene chloride, the occupancy of carbon atom is refined as 0.5, and chlorine atom as 1.0.

[K(222)][^{57}Fe(TPP)(CN)$_2$]. A dark purple, block crystal with the dimensions 0.38 × 0.20 × 0.19 mm was used for the structure determination. The asymmetric unit contains one-half porphyrin anion with required inversion symmetry and an ordered Kryptofix-222 molecule with 2-fold symmetry. No solvent molecule is found in the structure.

[K(222)][^{57}Fe(TMP)(CN)$_2$]·3CH$_2$Cl$_2$. A dark red crystal with the dimensions 0.46 × 0.38 × 0.07 mm was used for the structure determination. The asymmetric unit contains two half-porphyrin anions with required inversion symmetry and one ordered Kryptofix-222 molecule. There are two ordered methylene chloride solvent molecules. For the third disordered methylene chloride, both chlorine atoms were refined as two positions, and the C−Cl distances are constrained by means of DFIX commands.

[K(222)][^{57}Fe(TTP)(CN)$_2$]·2CH$_2$Cl$_2$. A dark purple, needle crystal with the dimensions 0.91 × 0.24 × 0.08 mm was used for the structure determination. The asymmetric unit contains one-half porphyrin anion with required inversion symmetry, one-half Kryptofix-222 molecule, and one-half methylene chloride solvent molecule, all of which are ordered.

RESULTS

The synthesis, molecular structures, and IR, EPR and Mössbauer spectroscopy of six new bis(cyano)iron(III) porphyrin complexes are reported. In a typical synthesis, the diaquo complex [Fe(TPP)(H$_2$O)$_2$]ClO$_4$,[24] sufficient KCN, and crown ether are reacted in methylene chloride solvent; after overnight stirring the dark solution was layered with hexanes to produce crystalline products.

The ν_{CN} stretches were determined in KBr pellets for all complexes: [K(18-C-6)][Fe(TPP)(CN)$_2$]·3.5CH$_2$Cl$_2$ (2115 cm^{-1}), [K(18-C-6)][Fe(TPP)(CN)$_2$]·3CH$_2$Cl$_2$ (2114 cm^{-1}), [K(222)][Fe(TPP)(CN)$_2$]·3.5CH$_2$Cl$_2$ (2114 cm^{-1}), [K(222)][^{57}Fe(TPP)(CN)$_2$] (2113 cm^{-1}), [K(222)][^{57}Fe(TMP)(CN)$_2$]·3CH$_2$Cl$_2$ (2113 cm^{-1}), and [K(222)][^{57}Fe(TTP)(CN)$_2$]·CH$_2$Cl$_2$ (2110 cm^{-1}).

Solid-state Mössbauer spectra were measured on several samples, including temperature-dependent measurements. Experimental results are given in Table 2. Values of the quadrupole splitting, isomer shift, line widths (full width at half-maximum, fwhm), and measurement temperature are tabulated. All measured spectra broaden as the temperature is lowered and the quadrupole doublet typically becomes less symmetric. Moreover, some of the lower temperature spectra cannot be readily fit to values for the quadrupole doublet and isomer shift; this is presumed to be the result of magnetic broadening. The values for the first six entries in the table are from this work; the next two have been reported previously from work in these laboratories.[16] To our knowledge, these Mössbauer spectra are the only ones observed from bis(cyano) complexes of known solid-state structure.

All complexes are low-spin $S = 1/2$, and ∼6 K EPR spectra have been measured for each species, both as ground single crystals and as frozen CH$_2$Cl$_2$ solutions. The EPR results are summarized in Table 3. Figures showing spectra will be displayed in the Discussion as appropriate.

The solid-state structures of six bis(cyano) iron(III) porphyrinates have been determined. Two crystalline forms of [K(18-C-6)][Fe(TPP)(CN)$_2$] have been studied: a block form, [K(18-C-6)][Fe(TPP)(CN)$_2$]·3.5CH$_2$Cl$_2$, and a needle form, [K(18-C-6)][Fe(TPP)(CN)$_2$]·3CH$_2$Cl$_2$. The environments of the two independent anions in the block form are distinctly different, as will be discussed subsequently. Labeled ORTEP diagrams of the full anions in both forms are given in Supporting Information Figures S1, S2, and S3.

Two crystalline forms of [K(222)][Fe(TPP)(CN)$_2$] have been determined. The structure of the first form, [K(222)][Fe(TPP)(CN)$_2$]·3.5CH$_2$Cl$_2$, shows that the two nitrogen atoms of the cyanide ligands have short contacts with solvent molecules (with the closest N···H distances of 2.366 and 2.386 Å). Although there are no solvent molecules in the second form, short contacts are found between the cyanide nitrogen atoms and surrounding hydrogen atoms. Labeled ORTEP diagrams for the [Fe(TPP)(CN)$_2$]$^-$ anions with K-222 are given in Supporting Information Figures S4 and S5.

In [K(222)][^{57}Fe(TMP)(CN)$_2$]·3CH$_2$Cl$_2$, both independent cyanide nitrogen atoms show short contacts with hydrogen atoms of the solvent methylene chloride (with N···H distances of 2.256 and 2.377 Å). Again in [K(222)][^{57}Fe(TTP)(CN)$_2$]·2CH$_2$Cl$_2$, the cyanide nitrogen atom shows short contacts with the hydrogen atom of methylene chloride (with a distance of N···H of 2.417 Å). Complete labeled ORTEP diagrams of the [Fe(TMP)(CN)$_2$]$^-$ anions are given in Supporting Information Figures S6 and S7, and that for [^{57}Fe(TTP)(CN)$_2$]$^-$ is given in Supporting Information Figure S8.

Table 4 summarizes the iron site symmetry and short cyanide nitrogen atom contacts with the crystalline environment. It can be seen that the bis(cyano) species easily forms structures with crystallographic required inversion centers, which is at least partially due to the cylindrical cyanide geometry. Short contacts are readily formed between the terminal cyanide and neighboring atoms, such as cations, solvents, and other groups, consistent with the partial negative charge on the cyano nitrogen atoms.

Formal 24-atom mean plane diagrams showing the displacement of atoms (in units of 0.01 Å) of all of the structures with required inversion symmetry are given in Figure 1. As can be expected, all displacements of iron centers are zero as a result of the inversion symmetry centers. The displacements of the 24 atoms are in the relatively small range from −0.10 to 0.10 Å. The diagrams also display the average values for each chemically unique type of bond length and bond angles. For the examples that have two independent porphyrins in one asymmetric unit, the difference in bond lengths and bond angles is small, and the

DOI: 10.1021/acs.inorgchem.5b00780
Inorg. Chem. 2015, 54, 6472−6485

Table 2. Mössbauer Parameters of Low-Spin Bis(cyano) Iron(III) Porphyrinates[a]

complex	phase	ΔE_q[b]	δ[b]	Γ(L)[b,c]	Γ(R)[b,c]	T (K)	ref
		$[Fe(Porph)(CN)_2]^-$					
$[K(18\text{-C-6})][Fe(TPP)(CN)_2]$	needle	1.79	0.12	0.58	0.54	100	tw
$\cdot 3CH_2Cl_2$	(microcrystalline)	1.55	0.15	0.50	0.44	200	tw
		1.04	0.06	0.44	0.39	298	tw
$[K(18\text{-C-6})][Fe(TPP)(CN)_2]$	block	no fit	no fit	very broad		15	tw
$\cdot 3.5CH_2Cl_2$	(microcrystalline)	1.00	0.16	1.49	0.98	50	tw
		1.98	0.15	0.62	0.73		tw
		0.69	0.22	0.75		100	tw
		1.77	0.11	0.60			tw
		0.67	0.18	0.61	0.50	150	tw
		1.70	0.11	0.43	0.44		tw
		0.67	0.18	0.49		200	tw
		1.71	0.11	0.46			tw
		0.48	0.11	0.36		295	tw
		1.12	0.05	0.36			tw
$[K(222)][Fe(TPP)(CN)_2]$	solid	0.61	0.40	0.33	0.32	100	tw
$\cdot 3CH_2Cl_2$	(microcrystalline)	0.61	0.37	0.31	0.31	200	tw
		0.62	0.29	0.34	0.32	298	tw
$[K(222)][^{57}Fe(TPP)(CN)_2]$	solid	no fit	no fit	very broad		4.2/9T	tw
$\cdot 3.5CH_2Cl_2$	(microcrystalline)	0.70	0.22	1.35	1.01	100	tw
		0.61	0.18	0.41	0.38	200	tw
		0.49	0.12	0.35	0.33	298	tw
$[K(222)][^{57}Fe(TMP)(CN)_2]$	solid			broad		4.2/1,3,9 T	tw
$\cdot 3CH_2Cl_2$	(microcrystalline)	no fit	no fit	very broad		50	tw
		0.50	0.20	0.57	0.64	100	tw
		0.40	0.16	0.28	0.29	200	tw
		0.35	0.09	0.26	0.28	298	tw
$[K(222)][^{57}Fe(TTP)(CN)_2]$	solid	0.66	0.09	0.32	0.39	298	tw
$\cdot 2CH_2Cl_2$	(microcrystalline)						
$[K((CH_3)_2CO)_2][Fe(TPP)(CN)_2]$	solid	−0.40[d]	0.19[d]	0.4		4.2	16
		no fit	no fit	very broad		15	16
		no fit	no fit	very broad		50	16
		−0.22	0.20	very broad		100	16
		−0.24	0.17	0.36	0.43	150	16
		−0.22	0.15	0.29	0.32	200	16
		−0.23	0.12	0.27	0.29	250	16
		−0.24	0.09	0.22	0.24	298	16
$[K(18\text{-C-6})][Fe(TMP)(CN)_2]$	solid	−1.25[e]	0.14[e]	0.5		4.2	16
		(−1.25[f])	no fit	very broad		15	16
		−1.27	0.16	1.24	0.82	50	16
		−1.15	0.16	0.70	0.55	100	16
		−1.09	0.16	0.56	0.47	200	16
		−0.82	0.12	0.39	0.34	250	16
		−0.68	0.10	0.34	0.29	298	16
$K[Fe(PPIX)(CN)_2]$	solution	−0.35	0.24			4.2	32
$K[Fe(TPP)(CN)_2]\cdot 2(CH_3)_2CO$	solid	0.63	0.31	0.50		78	33
$K[Fe(TTP)(CN)_2]\cdot 2(CH_3)_2CO$	solid	0.69	0.30	0.40		78	33
$Na[Fe(TPPS)(CN)_2]\cdot$bis DMF	solid	0.50	0.30	0.50		78	33
$Na[Fe(PPIX)(CN)_2]\cdot 3NaCN\cdot 6\ H_2O$	solid	0.53	0.20	0.48		80	34
		0.40	0.10	0.28		298	34
$K[Fe(PPIX)(CN)_2]$	solution	0.73	0.20	0.50		80	35
$[Fe(TPPS)] + xsCN^-$	solution	∼0	0.07	1.02		78	33

[a]Unless otherwise specified, measurements in low magnetic field. [b]In mm/s. [c]Line width at fwhm, L = left-hand line, R = right-hand line. [d]Value from fit to high-field spectra (5 and 9 T only). [e]Value from fit to high-field spectra (1, 5, 9 T). [f]Not observed, value from temperature-dependent fit.

values are not exceptional. Similar information for 24-atom mean plane diagrams of the remaining two structures, $[K(18\text{-C-6})][Fe(TPP)(CN)_2]\cdot 3.5CH_2Cl_2$ and $[K(222)][Fe(TPP)(CN)_2]$, with no required symmetry, is given in Figure 2. These structures show modest deformations from planarity that are a mixture of ruffling and saddling. The structure of $[K(222)][Fe(TPP)(CN)_2]$ was determined at 100 and 298 K. A comparison in the form of the formal cores is given in Supporting Information Figure S9; no substantial differences were noted, and the 298 K structure will not be discussed further. Distance and angle values found are reported as average values in the diagrams of Figures 1 and 2 and are unremarkable.[31]

DOI: 10.1021/acs.inorgchem.5b00780
Inorg. Chem. 2015, 54, 6472−6485

Table 3. EPR Parameters of Low-Spin Bis(cyano) Iron(III) Porphyrinates

complex	T (K)	phase[a]	g_{xx}	g_{yy}	g_{zz}	EPR type	ref
$[K(18\text{-}C\text{-}6)][Fe(TPP)(CN)_2]$	6.0	microcrystalline	2.55	2.55		axial[b]	tw
$\cdot 3CH_2Cl_2$(needle)		CH_2Cl_2			3.64	large g_{max}	
			2.50	2.50		axial	
$[K(18\text{-}C\text{-}6)][Fe(TPP)(CN)_2]$	6.0	microcrystalline		1.26	3.72	large g_{max}	tw
$\cdot 3.5CH_2Cl_2$(block)			2.55	2.55		axial[c]	
		CH_2Cl_2			3.64	large g_{max}	
			2.50	2.50		axial	
$[K(222)][^{57}Fe(TMP)(CN)_2]$	6.0	microcrystalline	2.55	2.55		axial	tw
$\cdot 3CH_2Cl_2$					3.76	large g_{max}	
		CH_2Cl_2	2.54	2.54		axial	
$[K(222)][Fe(TPP)(CN)_2]$	6.0	microcrystalline	2.55	2.55	1.13	axial	tw
$\cdot 3.5CH_2Cl_2$					3.83	large g_{max}	
		CH_2Cl_2			3.64	large g_{max}	
$[K(222)][^{57}Fe(TPP)(CN)_2]$	6.0	microcrystalline	2.55	2.55	1.13	axial	tw
					3.83	large g_{max}	
		CH_2Cl_2			3.64	large g_{max}	
$[K(222)][^{57}Fe(TTP)(CN)_2]$-	6.0	microcrystalline	2.55	2.55		axial	tw
$\cdot 2CH_2Cl_2$					3.83	large g_{max}	
		CH_2Cl_2			3.64	large g_{max}	
$[K((CH_3)_2CO)_2][Fe(TPP)(CN)_2]$	6.0	single crystal	0.52	1.05	3.70	large g_{max}	36
	4.2	CH_2Cl_2–CH_3OH			3.5	large g_{max}	16
		CH_2Cl_2–CH_3OH	1.76	2.2	2.74	rhombic	16
		microcrystalline			3.7	large g_{max}	16
$[K(18\text{- }C\text{-}6)][Fe(TMP)(CN)_2]$	4.2	CH_2Cl_2	2.54	2.54		axial	16
		microcrystalline	1.20	1.68	3.47	large g_{max}	16
$[Fe(PPIX)(CN)_2]^-$			1.03	2.42	3.75	large g_{max}	32
$[Fe(THP)(CN)_2]^-$	4.2	CH_2Cl_2–CH_3OH			3.5	large g_{max}	10
$[Fe(TPP)(CN)_2]^-$	4.2	CH_2Cl_2–CH_3OH			3.56	large g_{max}	11
$[Fe(OMTPP)(CN)_2]^-$	4.2	CH_2Cl_2			3.48	large g_{max}	37
$[Fe(OETPP)(CN)_2]^-$	4.2	CH_2Cl_2			3.31	large g_{max}	37
$[Fe(OETPP)(CN)_2]^-$					3.47	large g_{max}	38
$[Fe(OEP)(CN)_2]^-$					3.73	large g_{max}	38
$[Fe(TTP)(CN)_2]^-$[d]	4.2	CH_2Cl_2			3.6	large g_{max}	15
		CH_3OH	2.5	2.5		axial	15
$[Fe(TMP)(CN)_2]^-$			2.56	2.56	1.70	axial	38
$[Fe(TMP)(CN)_2]^-$[e]	4.2	CH_2Cl_2–CH_3OH	2.47	2.47	1.5	axial	11
$[Fe(T(Et_3P)P)(CN)_2]^-$[e]	4.2	CD_3OD	2.45	2.45	1.6	axial	14
$[Fe(TMeP)(CN)_2]^-$[f]	4.2	CH_2Cl_2–CH_3OH	2.43	2.43	1.69	axial	10
$[Fe(T^iPrP)(CN)_2]^-$[g]	4.2	CH_2Cl_2	2.42	2.42	1.74	axial	15
$[Fe(QTPP)(CN)_2]^-$[h]	77	CH_3OH	2.51	2.25	1.75	axial	39

[a] If two lines follow a phase in the table, both spectral types are seen in the same experiment. [b] Additional small signal at 2.87. [c] Additional small signal at 2.83. [d] Similar results were claimed for a number of *meso*-tetrakis(*p*-substituted-phenyl)porphyrin derivatives, *p*-X-TPP; X = OCH_3, H, F, Cl, $COOCH_3$, CF_3, and CN, but no data shown. [e] The complex shows either an axial type signal or both axial and large g_{max} type signals in different solvents.[14] Similar results for $[Fe(T(Et_3P)P)(CN)_2]^-$ and $[Fe(T(^iPr_3P)P)(CN)_2]^-$.[11] [f] Similar results were claimed for $[Fe(TEtP)(CN)_2]^-$ and $[Fe(T^iPrP)(CN)_2]^-$.[10] [g] Similar results were claimed for $[Fe(T^fPrP)(CN)_2]^-$ and $[Fe(T^nPrP)(CN)_2]^-$ without assigning g_{zz}.[13] [h] Similar results were claimed for $[Fe(MQTPP)(CN)_2]^-$ and $[Fe(PTPP)(CN)_2]^-$.[39]

Table 4. Summary of Iron Site Symmetry and Short Contacts of Cyanide Nitrogen Atoms

complex	nuclearity	Fe site sym	FeCN···X
$[K(18\text{-}C\text{-}6)][Fe(TPP)(CN)_2]$(b)	Fe1	C_i	K^+
	Fe2	C_i	H_{CH2Cl2}
$[K(18\text{-}C\text{-}6)][Fe(TPP)(CN)_2]$(n)	Fe1	C_1	K^+
$[K(222)][Fe(TPP)(CN)_2]$	Fe1	C_1	H_{CH2Cl2}
$[K(222)][^{57}Fe(TPP)(CN)_2]$	Fe1	C_i	H_R
$[K(222)][^{57}Fe(TMP)(CN)_2]$	Fe1	C_i	H_{CH2Cl2}
	Fe2	C_i	H_{CH2Cl2}
$[K(222)][^{57}Fe(TTP)(CN)_2]$	Fe1	C_i	H_{CH2Cl2}

DISCUSSION

Previously, we have studied the geometric and electronic structures of cyano iron(III) porphyrinate complexes including the mixed ligand species $[Fe(TPP)(CN)(Py)]$, $[Fe(TPP)(CN)(1\text{-}MeIm)]$, $[Fe(TMP)(CN)(1\text{-}MeIm)]$, and bis(cyano)species $K[Fe(TPP)(CN)_2]\cdot 2(CH_3)_2CO$ and $[K(18\text{-}C\text{-}6)][Fe(TMP)(CN)_2]$.[16,40−42] This work has led to our further interest in this topic, especially for the bis(cyano) species. Here, we report six new bis(cyano) porphyrinate complexes, which include four $[Fe(TPP)(CN)_2]^-$ structures, two each with $[K(18\text{-}C\text{-}6)]^+$ or $[K(222)]^+$ cations, and $[Fe(TMP)(CN)_2]^-$ and $[Fe(TTP)(CN)_2]^-$ structures with $[K(222)]^+$ cations. In this first section,

DOI: 10.1021/acs.inorgchem.5b00780
Inorg. Chem. 2015, 54, 6472−6485

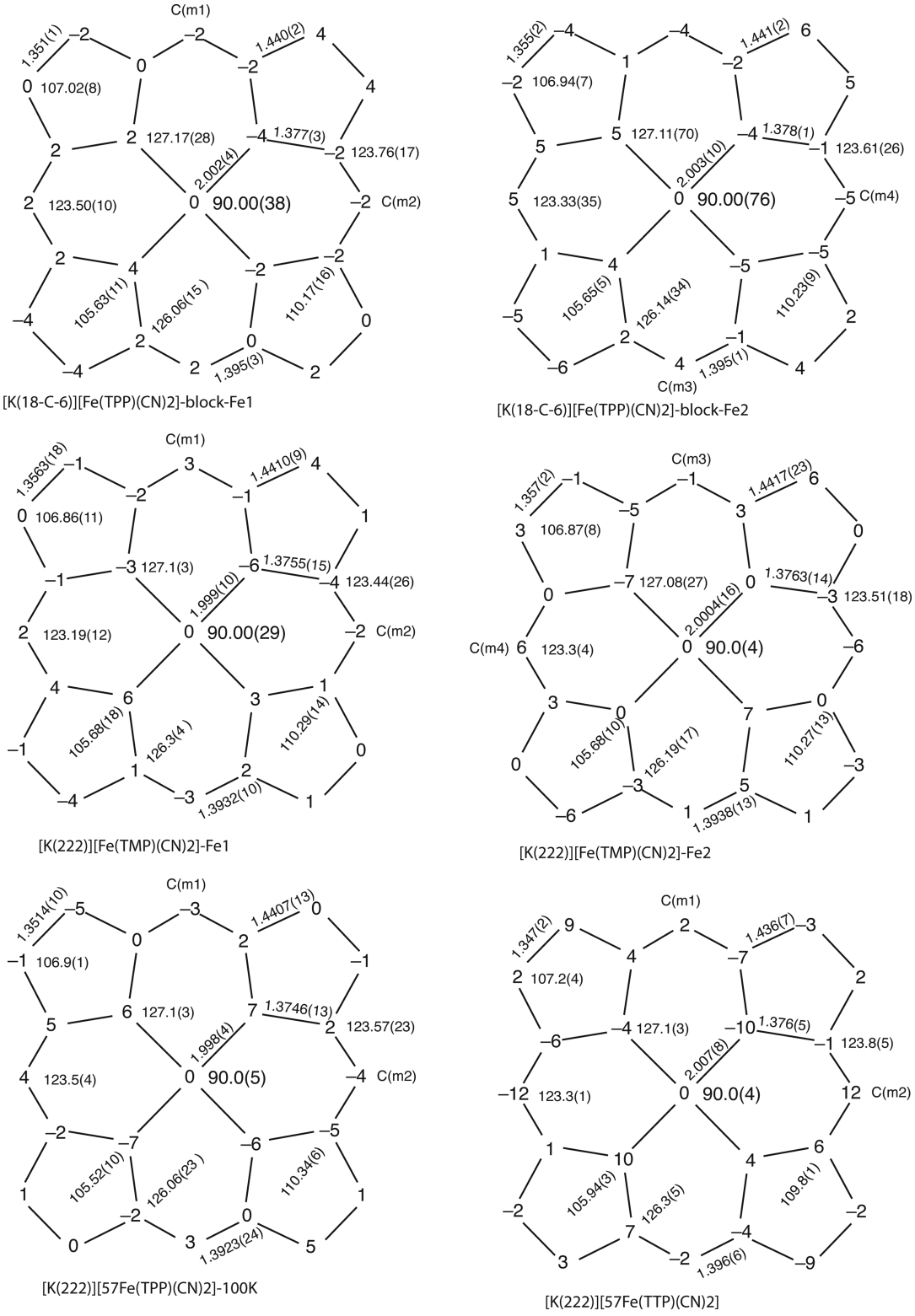

Figure 1. Formal diagrams of the porphyrin cores of $[K(18\text{-}C\text{-}6)][Fe(TPP)(CN)_2]\cdot 3.5CH_2Cl_2$, $[K(222)][^{57}Fe(TMP)(CN)_2]$, $[K(222)][^{57}Fe(TPP)(CN)_2]$, and $[K(222)][^{57}Fe(TTP)(CN)_2]\cdot 2CH_2Cl_2$; all anions have required inversion symmetry. The perpendicular displacements (in units of 0.01 Å) of the porphyrin core atoms from the 24-atom mean plane are displayed. Also displayed on the formal diagrams are the averaged values of the chemically unique bond distances (in Å) and angles (in degrees). The numbers in parentheses are the esd's calculated on the assumption that the averaged values were all drawn from the same population.

we emphasize the environment of the cyanide ligand in the solid-state structures.

Two $[Fe(TPP)(CN)_2]^-$ Structures with $[K(18\text{-}C\text{-}6)]^+$. We have determined two $[Fe(TPP)(CN)_2]^-$ structures with $[K(18\text{-}C\text{-}6)]^+$ cations, characterized by block or needle crystalline forms: $[K(18\text{-}C\text{-}6)][Fe(TPP)(CN)_2]\cdot 3.5CH_2Cl_2$ (block) and $[K(18\text{-}C\text{-}6)][Fe(TPP)(CN)_2]\cdot 3CH_2Cl_2$ (needle).

We first consider the block form structure. Two distinct iron sites are found (Figure 3): one (Fe 1:1, 0, 0) located at the corner of the unit cell, and the other (Fe2: 0.5, 0.5, 0.5) is at the unit cell

DOI: 10.1021/acs.inorgchem.5b00780
Inorg. Chem. 2015, 54, 6472−6485

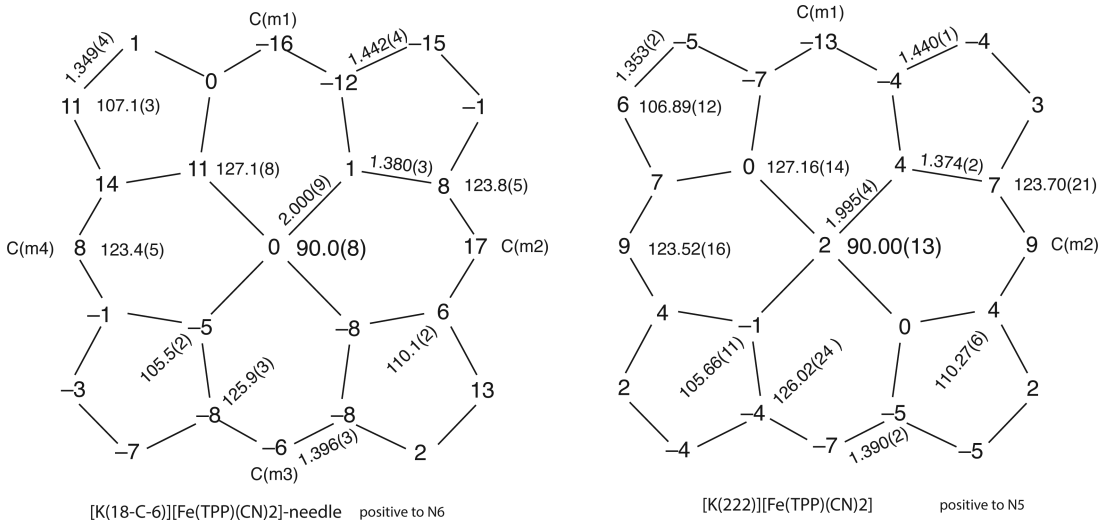

Figure 2. Formal diagrams of the porphyrin cores of $[K(18\text{-}C\text{-}6)][Fe(TPP)(CN)_2]\cdot 3CH_2Cl_2$ and $[K(222)][^{57}Fe(TPP)(CN)_2]$. The perpendicular displacements (in units of 0.01 Å) of the porphyrin core atoms from the 24-atom mean plane are displayed. Also displayed on the formal diagrams are the averaged values of the chemically unique bond distances (in Å) and angles (in degrees). The numbers in parentheses are the esd's calculated on the assumption that the averaged values were all drawn from the same population.

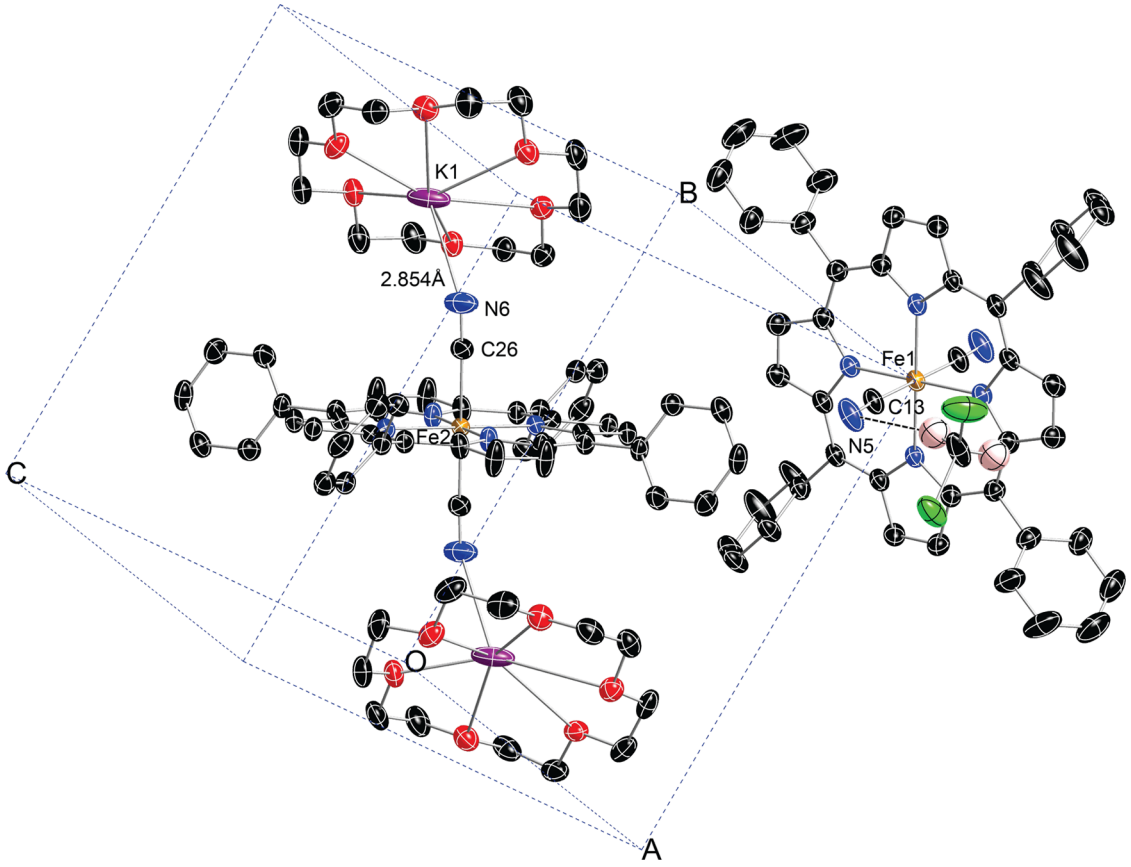

Figure 3. ORTEP diagram of $[K(18\text{-}C\text{-}6)][Fe(TPP)(CN)_2]\cdot 3.5CH_2Cl_2$ (block) displaying the atom labeling scheme and the two distinct iron sites. Thermal ellipsoids of all atoms are contoured at the 50% probability level. Hydrogen atoms have been omitted for clarity.

center. The two porphyrin cores are aligned near perpendicular with a dihedral angle of 100.7°. The iron located at the unit cell center interacts with the $[K(18\text{-}C\text{-}6)]^+$ cations through two identical K···N interactions (2.854(2) Å). The cyanide ligands thus form *exo*-bidendate coordination. Such *exo*-bidendate coordination has been seen in the ferric $[K(18\text{-}C\text{-}6)][Fe(TMP)(CN)_2]$[16] and ferrous $[K(222)]_2[Fe(TPP)(CN)_2]$[9] structures, where the K···N distances are 2.81(4) and 2.97(5) Å. The ~0.1 Å longer K···N distances in $[K(222)]_2[Fe(TPP)(CN)_2]$ may be due to the steric demands of the $[K(222)]^+$ cations. In the case of $[K((CH_3)_2CO)_2][Fe(TPP)(CN)_2]$ where the K^+ is stabilized by two acetone molecules, the K···N distance appears shorter (2.750(3) Å, Table 5). The second $[Fe(TPP)(CN)_2]^-$ anion has no contacts with the cation; however, it shows short contacts

DOI: 10.1021/acs.inorgchem.5b00780
Inorg. Chem. 2015, 54, 6472−6485

Table 5. Selected Structural Parameters for Bis(cyano) Iron Porphyrinates

complex	$(Fe-N_p)_{av}$[a]	Fe−C[a]	C−N[a]	N···K/H/Cu[b]	Fe−C−N[c]	C−N−G[c]	τ[c,d]	ν_{CN}[e]	ref
Bis(cyano) Iron(III) Porphyrinates									
$[K((CH_3)_2CO)_2][Fe(TPP)(CN)_2]$[f]	2.000(6)	1.975(2)	1.147(3)	2.750(3)[k]	177.8(3)	100.68(18)[k]	1.6	2120	41
[K(18-C-6)][Fe(TPP)(CN)$_2$][f,g](block)	2.002(4)	1.9808(19)	1.158(3)		176.6(2)		2.5	2115	tw
	2.003(10)	1.977(2)	1.154(3)	2.854(2)[k]	176.7(2)	155.2(2)[k]	3.9		tw
[K(18-C-6)][Fe(TPP)(CN)$_2$][g](needle)	2.000(9)	1.978(3)	1.162(4)	2.852(3)[k]	177.0(3)	143.8(2)[k]	6.0	2114	tw
		1.988(3)	1.152(4)	2.861(3)[k]	175.4(3)	142.2(3)[k]	7.5		tw
$[K(222)][Fe(TPP)(CN)_2]$[i]	1.995(4)	1.9773(18)	1.150(2)	2.366[l]	177.40(16)	113.7[l]	2.1	2114	tw
		1.9853(19)	1.146(3)	2.386[l]	175.47(16)	170.4[l]	3.4		tw
$[K(222)][^{57}Fe(TPP)(CN)_2]$[f] (100 K)	1.998(4)	1.9762(14)	1.151(2)	2.482[l]	173.34(13)		7.6	2113	tw
$[K(222)][^{57}Fe(TMP)(CN)_2]$[f,i]	1.999(10)	1.9865(13)	1.1565(18)	2.256[l]	174.87(12)	130.4[l]	5.5	2113	tw
	2.0004(16)	1.9841(17)	1.151(2)	2.377[l]	175.29(15)	122.4[l]	5.8		tw
$[K(222)][^{57}Fe(TTP)(CN)_2]$[f]	2.007(8)	1.985(2)	1.142(3)	2.417[l]	174.9(2)	102.2[l]	8.6	2110	tw
[K(18-C-6)][Fe(TMP)(CN)$_2$][g,h]	1.973(5)	1.970 (4)	1.158(1)		175.3(12)		3.8	2111	16
		1.986(6)	1.159(2)	2.81(4)[k,h]	172.8(14)	168.4(4)[k,h]	5.2		16
[PPN][Fe(TMP)(CN)$_2$][f]	2.003(4)	1.990 (5)	1.151(7)		178.6(5)				43
[K(222)][Fe(BH(Bipy)$_2$P)(CN)$_2$][j]	1.949(14)	1.949(4)	1.152(9)		170.8(5)		5.2		44
[Fe(OEOP)(CN)$_2$][f]	1.966(9)	1.969(10)	1.128(14)		177.4(11)		NR		45
Cyano Iron(II) Porphyrinates									
$[K(222)]_2[Fe(TPP)(CN)_2]$	1.990(4)	1.969(4)	1.157(5)		176.9(3)		1.7	2069	9
$[K(222)]_2[Fe(TTP)(CN)_2]$	1.999(6)	1.976(4)	1.159(5)		176.8(3)		3.8	2056	9
$[K(222)]_2[Fe(TPP)(CN)_2]$	1.974(11)	1.989(3)	1.160(3)	2.957(2)[k]	178.1(2)		0.8	2066	9
[K(222)][Fe(TPP)(CN)]	1.988(3)	1.929(3)	1.169(5)		176.6(3)		2.3	2076	9
[K(222)][Fe(TPP)(CN)](LS)	1.986(7)	1.8783(10)	1.1662(14)		177.19(10)		6.3	2070	8
[K(222)][Fe(TPP)(CN)](HS)	2.089(8)	2.108(3)	1.122(3)					2105	8
[K(222)][Fe(TPP)(1-MeIm(CN)](LS)	1.9835(8)	1.869(2)	1.152(3)		178.1(2)			2070	9
[K(222)][Fe(TPP)(1-MeIm(CN)](HS)	2.070(9)	2.068(4)	1.099(4)		176.5(4)				9
Bis(cyano)-Bridged Iron(III)−Copper(II) Porphyrinates									
$[(F_8\text{-TPP})Fe(CN)_2\{Cu(TMPA)\}_2]^{3+}$	1.973(4)[o]	1.98(2)	1.12(2)	1.89(1)[m]	173(2)	168(2)[m]	NR	2155	46
		1.98(2)	1.14(2)	1.92(1)[m]	177(2)	175(2)[m]	NR		
$[Cu(Me_6tren)]_2[Fe(OEP)(CN)_2]^{3+}$	1.995(1)	1.94(1)	1.14(2)	1.94(1)[m]	173(1)	171.89[m]	NR	2168, 2159	47
Bis(isocyano) Iron(III) Porphyrinates									
$[Fe(TPP)(t\text{-BuNC})_2]^+$	1.951(23)	1.928(22)	1.129(22)		174.8(9)	170.65[n]	NR	2200	48
		1.902(18)	1.117(20)		173.8(9)	176.29[n]	NR		
$[Fe(OEP)(t\text{-BuNC})_2]^+$	1.9769(13)	1.929(3)	1.145(4)		166.34(26)	166.45[n]	NR	2193	48
		1.925(3)	1.144(4)		169.80(26)	166.82[n]	NR		
$[Fe(TTP)(2,6\text{-xylylNC})_2]^+$	1.961(16)	1.95(1)	1.13(1)		172.8(9)	176.24[n]	NR	2195	49
		1.92(2)	1.16(1)		172.8(9)	175.03[n]	NR		
$[Fe(OMTPP)(t\text{-BuNC})_2]^+$	1.981(7)	1.909(12)	1.155		168.91	168.82[n]	NR	NR	50
		1.947(13)	1.163		171.71	171.98[n]	NR		
$[Fe(OMTPP)(t\text{-BuNC})_2]^+$	1.968(3)	1.932(5)	1.150		168.88	173.12[n]	NR	NR	50
		1.965(5)	1.140		168.67	176.86[n]	NR		

[a]Value in Å. [b]N···K, N···H, N···Cu distances, H is from the solvent CH_2Cl_2. [c]Value in degrees. [d]The tilt of Fe−C_{CN} vector from the normal to the 24-atom mean plane. [e]Value in cm^{-1}; KBr pellets. [f]These structures all have crystallographically required inversion symmetry. [g]Top line is for the simpler cyanide ligand/porphyrin unit, while the bottom line has cyanide further coordinated with K or H atoms. [h]Average values for the three unique [K(18-C-6)][Fe(TMP)(CN)$_2$] units. [i]Both cyanide groups have N···H(CH_2Cl_2). [j]Average values for the two cyanide groups. [k]N···K. [l]N···H. [m]N···Cu. [n]N−R. [o]Values are calculated from structural data in CCDC.

between the cyanide nitrogen atoms and the hydrogen of CH_2Cl_2 solvent molecules; for example, the N···H distance is 2.541 Å. The different coordination environments did not change the Fe−C−N angles, which are very similar at 176.6° and 176.7°.

In the needle form of $[K(18\text{-C-6})][Fe(TPP)(CN)_2]\cdot 3CH_2Cl_2$, the two cyanide nitrogen atoms interact with $[K(18\text{-C-6})]^+$ cations through two different K···N interactions (2.852(3) and 2.861(3) Å). An ORTEP diagram is given in Figure 4. This is different from the block form structure, where the two K···N interactions are the same because of crystallographic symmetry. The cyanide ligand of one [K(18-C-6)][Fe(TPP)(CN)$_2$] unit is bonded to the $[K(18\text{-C-6})]^+$ cation of the next molecule so as to form an infinite one-dimensional chain, which can be formulated as ···K−NC−Fe−CN···K−NC−Fe−CN···. A packing diagram of a portion of the cell is shown in the Supporting Information (Figure S10). It is seen that the one-dimensional chain is helical. The porphyrin core is moderately distorted with both ruffling and saddling characteristics. The C(m1) (−0.16 Å) and C(m2) (0.17 Å) atoms show the largest deviation in opposite directions.

Two $[Fe(TPP)(CN)_2]^-$ Structures with $[K(222)]^+$. The second type of $[Fe(TPP)(CN)_2]^-$ structures is those with the $[K(222)]^+$ cation, which have formulas $[K(222)][Fe(TPP)(CN)_2]\cdot 3.5CH_2Cl_2$ and $[K(222)][^{57}Fe(TPP)(CN)_2]$ (Figure 5). In $[K(222)][Fe(TPP)(CN)_2]\cdot 3.5CH_2Cl_2$, both cyanide groups

DOI: 10.1021/acs.inorgchem.5b00780
Inorg. Chem. 2015, 54, 6472−6485

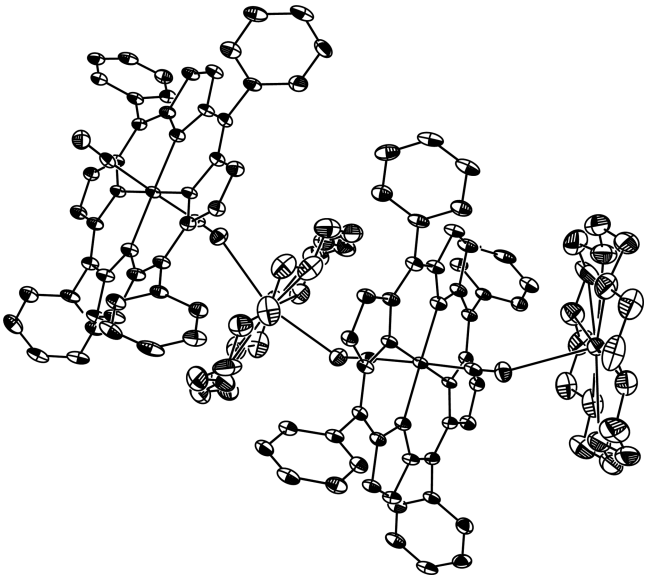

Figure 4. ORTEP diagram of the iron environment in the needle form of $[K(18\text{-}C\text{-}6)][Fe(TPP)(CN)_2]\cdot 3CH_2Cl_2$. Thermal ellipsoids of all atoms are contoured at the 50% probability level. Hydrogen atoms have been omitted for clarity.

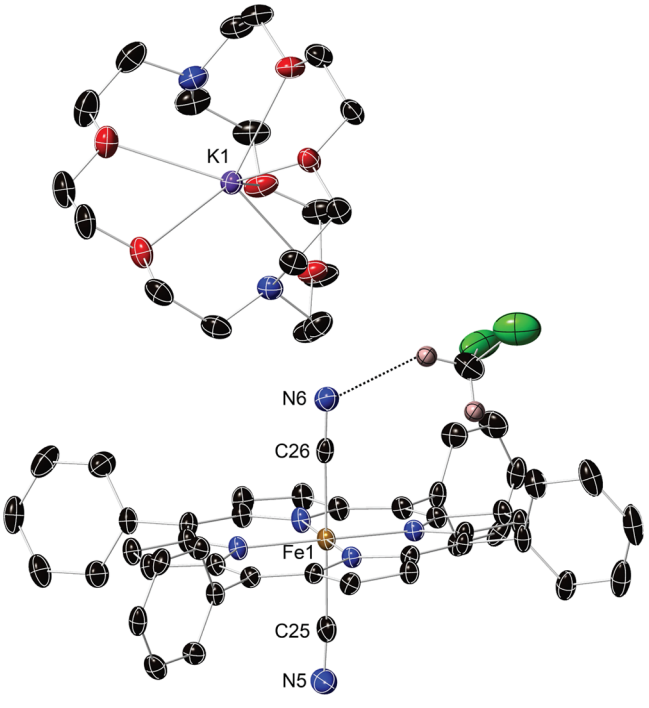

Figure 5. ORTEP diagram of $[K(222)][Fe(TPP)(CN)_2]\cdot 3.5CH_2Cl_2$ displaying the atom labeling scheme. Thermal ellipsoids of all atoms are contoured at the 50% probability level. Hydrogen atoms have been omitted for clarity.

show short N···H interactions with CH_2Cl_2 solvent; for example, the N6···H distance is 2.367 Å. A typically ruffled porphyrin ring is seen in the 24-atom mean plane (Figure 2), with the deviation of the *meso* carbons from the 24-atom mean plane, $|\Delta C_m| = 0.10$ Å. The displacement of the iron center is 0.02 Å directed to N5. Although the second crystalline form does not have any solvent for possible interaction with the nitrogen atom of the cyanide, it does have short N···H interactions (2.482 Å) with adjacent porphyrin molecules.

$[K(222)][^{57}Fe(TMP)(CN)_2]$ and $[K(222)][^{57}Fe(TTP)(CN)_2]$ Structures. $K(222)][^{57}Fe(TMP)(CN)_2]$ has two distinct iron sites as shown in Figure 6. Unlike $[K(18\text{-}C\text{-}6)][Fe(TPP)(CN)_2]$, the cyanide nitrogen atoms of both sites interact with a hydrogen atom of CH_2Cl_2 and not a K^+ ion. The two porphyrin planes are roughly perpendicular with a dihedral angle of 80.5°.

The cyanide nitrogen atom in $[K(222)][^{57}Fe(TTP)(CN)_2]\cdot 2CH_2Cl_2$ interacts with a hydrogen atom of the solvent with a N···H interaction distance of 2.417 Å.

Other Structural Issues. Selected structural parameters of bis(cyano) iron(III)porphyrinates are reported in Table 5. We first consider the averaged Fe−N_p distances. The range of distances for the present complexes, 1.973(5)−2.003(10) Å, is well within the range expected for low-spin iron(III) species.[51] $[K(222)][Fe(BH(Bipy)_2P)(CN)_2]$ and $[Fe(OEOP)(CN)_2]$ show shorter distances; the difference is explained by the highly hindered basket-handle porphyrin $(BH(Bipy)_2P)$[44] and oxygen substituted octaethyloxoporphyrin (OEOP).[45] These shorter Fe−N_p distances are consistent with the significantly ruffled core.[48−50] The steric effects of the strap in $[K(222)][Fe(BH(Bipy)_2P)(CN)_2]$ also induce the shortest Fe−C(CN) bond distance of 1.949(4) Å. The remaining Fe−C(CN) bond distances are in the range of 1.970−1.987 Å.

Table 5 also presents structural data for the known iron(II) cyano derivatives. The values of the Fe−N_p and Fe−C distances for the bis(cyano) iron(II) species are within the same range of values as for the iron(III) derivatives. The corresponding values for the low- and high-spin forms of the five-coordinate derivatives are, not surprisingly, different with the low-spin Fe−C distances shorter and the high-spin distances longer. The Fe−N_p distances for the high-spin iron(II) states are much larger as expected.

For further comparison, selected structural parameters of (cyano)-bridged iron(III)−copper(II) and bis(isocyano) iron(III) porphyrinate complexes are also given in Table 5. The bis(isocyano) complexes present quite short Fe−N_p distances, consistent with their significantly ruffled cores.[48−50] This compares to the corresponding distance of 1.973(5) Å in $[K(18\text{-}C\text{-}6)][Fe(TMP)(CN)_2]$ and 1.973(4) Å in $[(F_8\text{-}TPP)Fe(CN)_2\{Cu(TMPA)\}_2]^{3+}$, both of which also show strongly ruffled conformations. It is known that core ruffling and short M−N_p bonds are tightly coupled parameters, with core ruffling leading to shortened M−N_p bonds.[52]

As compared to the bis(cyano) and the bis(cyano)-bridged iron(III)−copper(II) complexes, the isocyanide analogues show shorter Fe−C distances in the range of 1.902−1.965 Å. This is explained by the bonding property that the isocyanide ligand would display some carbene character when bound to the metal center: Fe−C≡N(R) ↔ Fe=C=N(R).[53]

The porphyrin complexes present three kinds of interactions for N···K/H/Cu and are listed in Table 5. It is seen that the three kinds of interaction have the following sequence in length: N−Cu (coordinate bond) < N···H (weak interaction) < N···K (intermolecular interaction/ion-dipole interaction). The N−Cu distances in the bis(cyano)-bridged iron(III)−copper(II) porphyrin structures range from 1.89−1.94 Å, which are typical N(CN)−Cu(II) distances for analogues like $[(Py)(OEP)Fe(CN)Cu(Npy_3)]^{2+}$ (1.906(8) Å),[47] $[(Py)(OEP)Fe(CN)Cu(Me_6tren)]^{2+}$ (1.988(1) and 1.91(1) Å),[54] and $[(Py)(F_8\text{-}TPP)Fe(CN)Cu(TMPA)]^{2+}$ (1.945(6) Å).[46] The Fe−C−N angles are essentially linear ranging from 173° to 177°.

Both N···H and N···K noncovalent intermolecular interactions are observed in bis(cyano) complexes with the N···K distance

DOI: 10.1021/acs.inorgchem.5b00780
Inorg. Chem. 2015, 54, 6472−6485

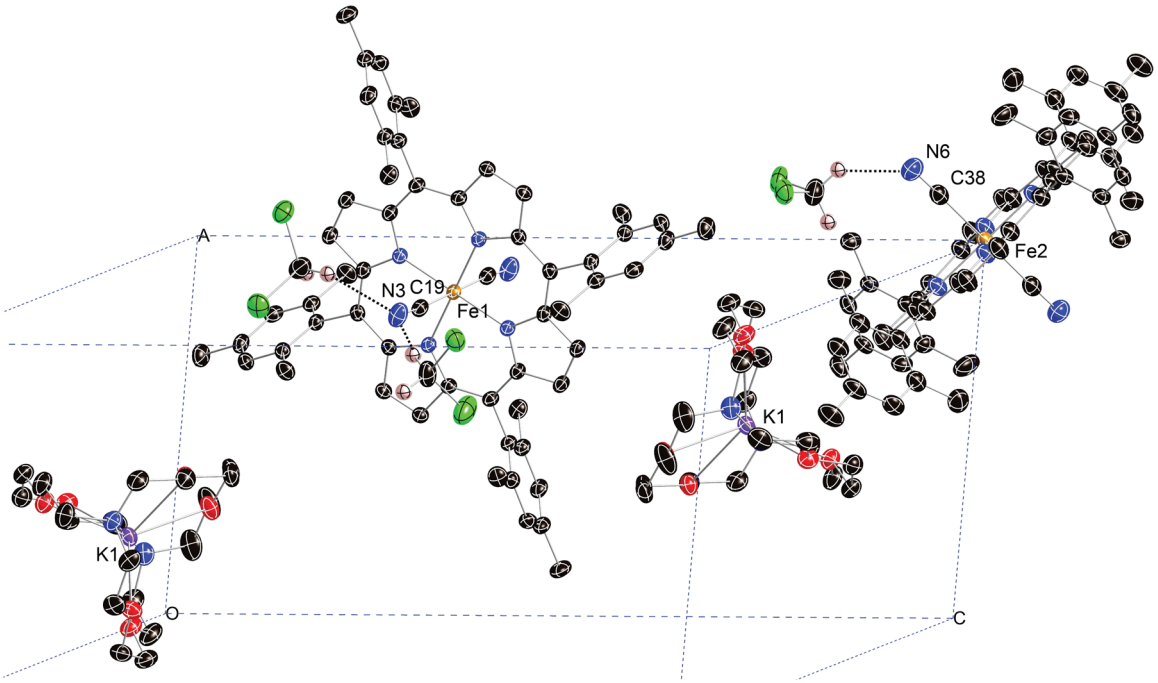

Figure 6. ORTEP diagram of $[K(222)][^{57}Fe(TMP)(CN)_2]\cdot 3CH_2Cl_2$ displaying the atom labeling scheme. Thermal ellipsoids of all atoms are contoured at the 50% probability level. Hydrogen atoms have been omitted for clarity.

relatively longer than N···H interactions. The Fe−C−N angles are found in a broad range of 170.8(5)°−178.6(5)°. Again, the most bent Fe−C−N angle (170.8(5)°) is derived from the highly hindered basket-handle porphyrin complex[K(222)][Fe(BH-(Bipy)$_2$P)(CN)$_2$]. The most linear Fe−C−N groups (≥177.4°) are found in the structures with crystallographically required symmetry such as $[K((CH_3)_2CO)_2][Fe(TPP)(CN)_2]$ (177.8°), [PPN][Fe(TMP)(CN)$_2$] (178.6°), and [Fe(OEOP)(CN)$_2$] (177.4°).

The tilt angles of the Fe−C_{CN} vector from the normal to the 24-atom mean plane are also given in Table 5. In the structures where there are N···K interactions, the interaction always induced larger τ angles as compared to the other Fe−C_{CN} vector. This is the case of [K(18-C-6)][Fe(TPP)(CN)$_2$](needle) and [K(18-C-6)][Fe(TMP)(CN)$_2$]. In both structures, only one of the two cyanide groups has an N···K interaction, and this cyanide group leads to a observable big τ angle (7.5 to 6.0; 5.2 to 3.8). However, some structures without any N···K interaction also show large τ angles. This is seen in the structures of [K(222)][Fe(TPP)-(CN)$_2$] and [K(222)][Fe(TTP)(CN)$_2$], both of which have required inversion symmetry and show angles ≥7.6°.

C−N Stretching Frequency. The C−N stretch has been proven to be a useful monitor of the bonding sites and ligand environment for both hemoproteins and porphyrinates.[16,55−59] We have shown that the C−N stretching frequency of the dicyano derivatives $K[Fe(TPP)(CN)_2]\cdot 2(CH_3)_2CO$ (2120 cm^{-1}) and [K(18-C-6)][Fe(TMP)(CN)$_2$] (2111 cm^{-1}) shifts to higher frequency by 10−14 cm^{-1} when the *trans*-cyanide is replaced by pyridine ([Fe(TPP)(CN)(Py)], 2130 cm^{-1}) or 1-MeIm ([Fe(TPP)(CN)(1-MeIm)], 2130 cm^{-1}, [Fe(TMP)(CN)(1-MeIm)], 2125 cm^{-1}).[16] The C−N stretching band for these six new bis(cyano) complexes is similarly weak. The C−N frequencies are $[K(18\text{-}C\text{-}6)][Fe(TPP)(CN)_2]\cdot 3.5CH_2Cl_2$ (2115 cm^{-1}), $[K(18\text{-}C\text{-}6)][Fe(TPP)(CN)_2]\cdot 3CH_2Cl_2$ (2114 cm^{-1}), [K(222)][Fe(TPP)(CN)$_2$] (2114 cm^{-1}), [K(222)][^{57}Fe(TPP)-(CN)$_2$] (2113 cm^{-1}), [K(222)][^{57}Fe(TMP)(CN)$_2$] (2113 cm^{-1}), and [K(222)][^{57}Fe(TTP)(CN)$_2$] (2110 cm^{-1}). As expected, these values are in accord with our previous results, which confirms again that bis(cyano) complexes show lower frequencies as compared to mixed-ligand complexes because of the change in the σ-acceptor behavior of iron(III).[16] The C−N frequencies for all iron(II) derivatives are found at lower frequencies (Table 5).

Mössbauer Spectra. Solid-state Mössbauer spectral measurements have been made on the bis(cyanide) complexes, including temperature-dependent measurements. Most of the bis-cyanide complexes show strong temperature-dependence of the quadrupole splitting with the two crystalline forms of [K(18-C-6)]-[Fe(TPP)(CN)$_2$] and [K(18-C-6)][Fe(TMP)(CN)$_2$] showing the largest range of values. This large temperature-dependence of the quadrupole splitting pattern is strongly suggestive of the presence of low-lying excited states. Indeed, the totality of the Mössbauer and EPR observations is consistent with small energy differences between the $(d_{xz},d_{yz})^4(d_{xy})^1$ and the $(d_{xy})^2(d_{xz},d_{yz})^3$ states. Small differences in either the porphyrin ligand or the environment of the bis(cyanide) anion is sufficient to tilt in favor of one state or the other. The symmetric π-bonding ability of the cyanide ligands stabilizes both d_π (d_{xz} and d_{yz}) orbitals leading to either near-equal energies (and the $(d_{xy})^2(d_{xz},d_{yz})^3$ state). Alternatively, the two d_π orbitals can be sufficiently stabilized so that their energies are below that of the d_{xy} orbital leading to the $(d_{xz},d_{yz})^4(d_{xy})^1$ state. This model of cyanide bonding is consistent with the isomer shift values at room temperature of ∼0.09−0.12 mm/s, smaller than those found for "classical" low-spin iron(III) porphyrinates, but consistent with strong Fe−CN covalency. In principle, the two electronic states should be distinguishable from the sign of the quadrupole splitting.[60] Determining the sign requires measurements in high applied magnetic field. One such measurement, that for [K(222)][^{57}Fe(TPP)(CN)$_2$], gave spectra too broad for interpretation. Spectra for [K(222)][^{57}Fe(TMP)(CN)$_2$] could be fit with either sign and plausibly are the result of species with both signs present. This is consistent with the site symmetry and the observation of two types of EPR spectra in the solid.

DOI: 10.1021/acs.inorgchem.5b00780
Inorg. Chem. 2015, 54, 6472−6485

The quadrupole splitting values are seen to be sensitive to the solid-state environment of the $[Fe(porph)(CN)_2]^-$ ions. This is most evident for the two crystalline forms of $[K(18\text{-}C\text{-}6)][Fe(TPP)(CN)_2]$. The "block" form has one centrosymmetric $[Fe(TPP)(CN)_2]^-$ anion with two equivalent K···N interactions at distances of 2.854(2) Å forming a tight ion pair with the $[K(18\text{-}C\text{-}6)]^+$ cations. The second centrosymmetric $[Fe(TPP)(CN)_2]^-$ anion has no close contacts with other atoms in the crystal. Accordingly, we would expect to see two distinct Mössbauer quadrupole doublets, which are in fact observed. A spectrum of the block form of $[K(18\text{-}C\text{-}6)][Fe(TPP)(CN)_2]$ is shown in Figure 7. The two doublets are sufficiently

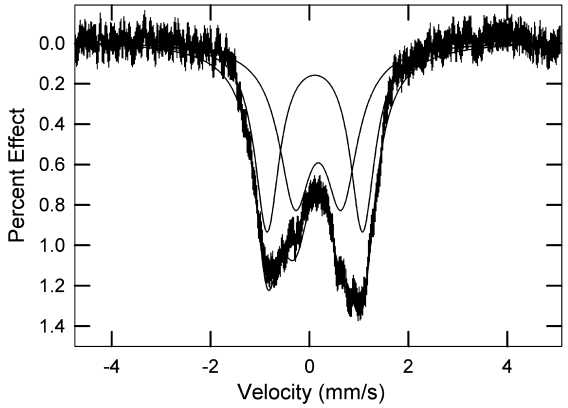

Figure 7. Mössbauer spectra at 100 K for $[K(18\text{-}C\text{-}6)][Fe(TPP)(CN)_2]$ (block) showing the two overlapped quadrupole split doublets and the deconvolution.

overlapped that providing exact values is challenging. Nonetheless at 100 K, the two sets of values are 1.93 mm/s for ΔE_q and 0.12 mm/s for the isomer shift and 0.93 mm/s for ΔE_q and 0.17 mm/s for the isomer shift. The higher set of values should be assigned to the ion-paired anion; this is consistent with the 1.79 mm/s for ΔE_q and 0.12 for the isomer shift for "needle" form of $[K(18\text{-}C\text{-}6)][Fe(TPP)(CN)_2]$ (also at 100 K). Note the agreement with the observed solid-state structure of two K···N interactions in this crystalline form. Interestingly, we had previously observed[16] ΔE_q = 1.15 mm/s and an isomer shift of 0.16 mm/s for $[K(18\text{-}C\text{-}6)][Fe(TMP)(CN)_2]$, values intermediate to the pair above. This derivative has only one of the two cyanide ligands involved in a K···N interaction, again pointing out the importance of cyanide ligand environment on the values of the Mössbauer spectrum.

From these observations, we see that the magnitude of Mössbauer quadrupole splitting can lead to the assignment of the environment of the cyanide ligand(s) in the bis(cyanide) complexes. The simple correlation in values of ΔE_q = 1.7−1.9 mm/s corresponds to species with both cyanides having N···K interactions, $\Delta E_q \approx$ 1.25 mm/s corresponds to species with one cyanide having N···K interactions, and $\Delta E_q \approx$ 0.60−0.90 mm/s corresponds to species with no cyanide ligand having N···K interactions. The application of this correlation to the remaining four derivatives characterized in this Article predicts the correct environment for all, no interaction with the cation.

Finally, we do note that there is one counterexample, that of the $[K((CH_3)_2CO)_2]][Fe(TPP)(CN)_2]$ complex, which is observed to have ΔE_q values of ∼0.25 mm/s and minimal temperature variation. The geometry around the K^+ is extremely unusual, with an extremely low coordination number for potassium (4) formed by the two acetone oxygen donors and two nitrogen atom donors formed from the bridging of two cyanides from adjacent porphyrin anions. This leads to a distinctly different C−N···K geometry. The group has a C−N−K angle of 100°; the other interactions of this type have angles of 140−150°.

The assignment of individual ground states to the $[Fe(TPP)(CN)_2]$ anions and further insight into their electronic structure are greatly assisted by the complementary application of EPR spectroscopy.

EPR Spectra. There are three types of EPR spectra that have been observed for low-spin iron(III) porphyrinates; all can be correlated with structural features and a specific ground-state electronic structure. Normal rhombic EPR spectra with three g values (2.8−2.9, 2.2−2.4, and 1.5−1.6) are typically observed for iron(III) porphyrinates with pyridine or imidazole ligands that have a coplanar arrangement of the axial ligands. This type of EPR spectrum is also commonly seen in heme proteins including those with mixed axial ligands. The observation of a rhombic EPR spectrum is clear evidence for the $(d_{xy})^2(d_{xz})^2(d_{yz})^1$ configuration where the d_{yz} orbital is conventionally taken as the singly occupied orbital. The energy difference between the d_{xz} and d_{yz} orbitals is on the order of 2−3 times the value of the spin orbit coupling constant or 600−1000 cm^{-1}.[61,63] A second type of EPR spectrum with a single feature EPR spectrum and g value ≥3.3 is known as the "large g_{max}"[61] or "HALS".[64,65] This spectral type is correlated with complexes with the two axial ligands having a relative perpendicular orientation.[61,62,66,67] This geometrical feature leads to very small splitting between the d_{xz} and d_{yz} orbitals, less than the value of the spin-orbit coupling constant or ≪400 cm^{-1}. The electronic structure can thus be expressed as $(d_{xy})^2(d_{xz},d_{yz})^3$. The observation of this signal requires measurement temperatures below about 20 K. All three components of the g-tensor can typically only be observed in oriented single crystal measurements. This EPR signal has been seen in a number of mitochondrial-bound cytochromes, including initially cytochrome bc_1.[68,69] A third type of EPR spectrum results from the coordination of weak σ-bonding, π-accepting ligands such as 4-CNPy[70] or isocyanides.[48] This spectral type is "axial" with one line above g = 2 and one below. This EPR spectral type results from the electronic structure $(d_{xz},d_{yz})^4(d_{xy})^1$.

We have obtained EPR spectra on crushed single crystals (microcrystalline) and frozen CH_2Cl_2 glass samples. The results of these measurements are listed in Table 3. At first glance, the observations may appear overly complex, but we believe that they provide crucial insight into the character of the bis(cyanide) complexes. The combination of both solid-state and solution measurements is essential. The spectral components are either of the large g_{max} or axial type. The cylindrical nature of the cyanide ligand does not lead to any orientational effects, and we do not find any evidence that porphyrin core ruffling is absolutely needed for observation of the axial EPR spectrum as suggested by Nakamura and Fujii.[11]

We begin our analysis by considering the two crystalline forms of $[K(18\text{-}C\text{-}6)][Fe(TPP)(CN)_2]$. In the solid state, the block form, with its two distinct iron sites, displays both a large g_{max} and an axial spectrum. The needle form, on the other hand, displays only an axial spectrum. The frozen solution spectra of both forms display identical spectra with both an axial and a large g_{max} signal apparent. We believe that this is because the two electronic states that give rise to the two spectral types are very close in energy and both are frozen out in making the CH_2Cl_2 glass. Note that these two complexes showed the largest (and large)

DOI: 10.1021/acs.inorgchem.5b00780
Inorg. Chem. 2015, 54, 6472−6485

temperature-dependence of the quadrupole splitting values, implying the closest low-lying excited states. These spectra are illustrated in Figures 8 and 9. Other EPR spectra are given in the Supporting Information.

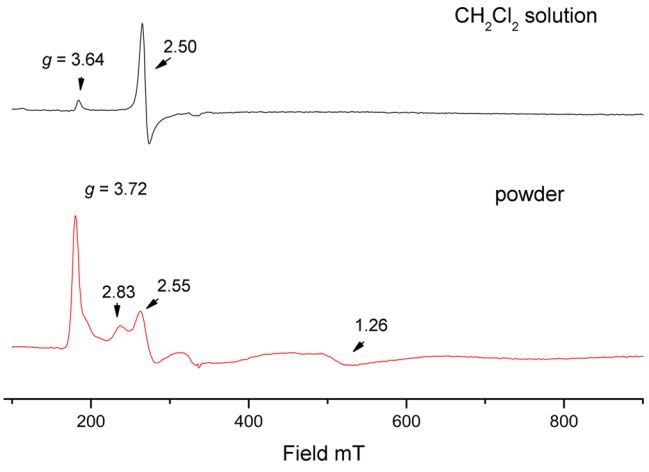

Figure 8. Solid-state and frozen solution EPR spectra for the block form of $[K(18\text{-}C\text{-}6)][Fe(TPP)(CN)_2]\cdot 3.5CH_2Cl_2$.

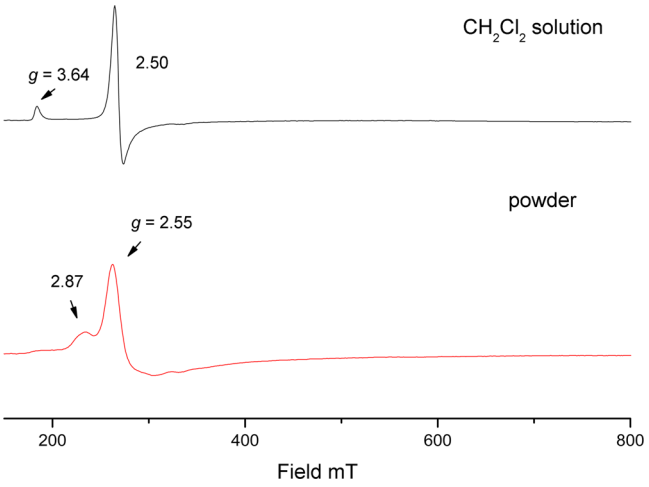

Figure 9. Solid-state and frozen solution EPR spectra for the needle form of $[K(18\text{-}C\text{-}6)][Fe(TPP)(CN)_2]\cdot 3CH_2Cl_2$.

Possible confirming data are given by the solid-state spectra of $[K(222)][Fe(TMP)(CN)_2]$. This molecule, in the solid state, has two sites that are structurally similar, and yet both spectral types are seen in the solid-state spectrum, again consistent with small energy differences between the two possible electronic states. The three remaining derivatives all display both an axial and a large g_{max} signal in the solid state. It is possible that one of these solid-state components is a minor component; integration of these signals cannot be used for estimations of the relative amounts because the short relaxation times make the large g_{max} signal appear much smaller. A single large g_{max} type signal in frozen CH_2Cl_2 is observed for all three. Table 3 also lists EPR observations from a number of other investigators. All of these measurements were made in various frozen solutions or on solids of unknown solid-state structure. However, none of the measurements would contravene the conclusions reached above.

SUMMARY

Six different bis(cyano) iron(III) porphyrinates, with varying counterions and porphyrin ligands, have been characterized by X-ray crystal structures, solid-state Mössbauer, and solid-state and frozen solution EPR spectroscopy. The complexes display two different electronic structures; the spectroscopic studies are consistent with small energy differences between the $(d_{xz},d_{yz})^4(d_{xy})^1$ and the $(d_{xy})^2(d_{xz},d_{yz})^3$ states. In addition to the effects of varying the porphyrin ligand, subtle effects of the cyanide ligand environment (the interaction of the nitrogen atom of the cyanide with its surroundings) in the solid state and in solution are sufficient to shift the balance between the two.

ASSOCIATED CONTENT

Supporting Information

Figures S1−S13: ORTEP diagrams and EPR spectra. Tables S1−S42: Complete crystallographic details, atomic coordinates, bond distances and angles, anisotropic temperature factors, and fixed hydrogen atom positions for all structures reported. Crystallographic information files (CIF) are also available. The Supporting Information is available free of charge on the ACS Publications website at DOI: 10.1021/acs.inorgchem.5b00780.

AUTHOR INFORMATION

Corresponding Authors

*E-mail: jfli@ucas.ac.cn.
*E-mail: cshulz@knox.edu.
*E-mail: scheidt.1@nd.edu.

Notes

The authors declare no competing financial interest.

ACKNOWLEDGMENTS

Research reported in this publication was supported by the CAS Hundred Talent Program and National Natural Science Foundation of China (Grant no. 21371167) to J.L., and the National Institutes of Health under Grant GM-38401 to W.R.S. W.R.S. acknowledges a CAS Professorship for Senior International Scientists. We also thank the U.S. National Science Foundation for EPR support through instrumentation grant NSF-98-70990. We thank Dr. Allen Oliver for assistance in organizing the X-ray data.

REFERENCES

(1) (a) Wilson, D. F.; Erecinska, M. In *Methods in Enzymology*; Fleischer, S., Leaster, P., Eds.; Academic Press: New York, 1978; Vol. *53*, pp 191−197. (b) Erecinska, M.; Wilson, D. F.; Sato, N.; Nicholls, P. *Arch. Biochem. Biophys.* **1972**, *151*, 188.

(2) Nicholls, P.; Vanburen, K. J. H.; Gelder, B. F. V. *Biochim. Biophys. Acta* **1972**, *275*, 279.

(3) Curry, S. C.; LoVecchio, F. A. Hydrogen Cyanide and Inorganic Cyanide Salts. In *Clinical Environmental Health and Toxic Exposures*; Sullivan, J. B., Krieger, G. R., Eds.; Lippincott, Williams & Wilkins: Philadelphia, PA, 2001; pp 705−716.

(4) Antonini, E.; Brunori, M. *Hemoglobin and Myoglobin in Their Reactions with Ligands*; North-Holland: Amsterdam, London, 1971.

(5) Solomonson, L. P. In *Cyanide in Biology*; Vennesland, B., Conn, E. E., Knowles, C. J., Westley, J., Wissing, I., Eds.; Academic Press: New York, 1981; pp 11−28.

(6) (a) Moreno, S. N. J.; Stolze, K.; Janzen, E. G.; Mason, R. P. *Arch. Biochem. Biophys.* **1988**, *265*, 267.

(7) Stolze, K.; Moreno, S. N. J.; Mason, R. P. *J. Inorg. Biochem.* **1989**, *37*, 45.

(8) Li, J.; Lord, R. L.; Noll, B. C.; Baik, M.-H.; Schulz, C. E.; Scheidt, W. R. *Angew. Chem., Int. Ed.* **2008**, *47*, 10144.

DOI: 10.1021/acs.inorgchem.5b00780
Inorg. Chem. 2015, 54, 6472−6485

(9) Li, J.; Noll, B. C.; Schulz, C. E.; Scheidt, W. R. *Angew. Chem., Int. Ed.* **2009**, *48*, 5010.
(10) Nakamura, M.; Ikeue, T.; Fujii, H.; Yoshimura, T. *J. Am. Chem. Soc.* **1997**, *119*, 6284.
(11) Nakamura, M.; Ikeue, T.; Ikezaki, A.; Ohgo, Y.; Fujii, H. *Inorg. Chem.* **1999**, *38*, 3857.
(12) Nakamura, M.; Ikeue, T.; Fujii, H.; Yoshimura, T.; Tajima, K. *Inorg. Chem.* **1998**, *37*, 2405.
(13) Ikeue, T.; Ohgo, Y.; Saitoh, T.; Nakamura, M.; Fujii, H.; Yokoyama, M. *J. Am. Chem. Soc.* **2000**, *122*, 4068.
(14) Ikezaki, A.; Nakamura, M. *Inorg. Chem.* **2002**, *41*, 2761.
(15) Ikezaki, A.; Ikeue, T.; Nakamura, M. *Inorg. Chim. Acta* **2002**, *335*, 91.
(16) Li, J.; Noll, B. C.; Schulz, C. E.; Scheidt, W. R. *Inorg. Chem.* **2007**, *46*, 2286.
(17) Abbreviations: Porph, generalized porphyrin dianion; BH(Bipy)$_2$P, bis(6,6′-diphenylbipyridine) basket-handle porphyrin dianion; MQTPP, (methylquinoxalino)tetraphenylporphyrin dianion; OEP, 2,3,7,8,12,13,17,18-octaethylporphyrin dianion; OEOP, octaethyloxoporphyrin dianion; ORTPP (R = M or E), dianion of 2,3,7,8,12,13,17,18-octaalkyl-5,10,15,20-tetraphenylporphyrin where R is methyl (M) or ethyl (E); PPIX, protoporphyrin IX dianion; QTPP, quinoxalinotetraphenylporphyrin dianion; PTPP, pyrazinotetraphenylporphyrin dianion; T(Et$_3$P)P, *meso*-tetrakis(2,4,6-triethylphenyl)-porphyrin; THP, porphine dianion; TMP, *meso*-tetramesitylporphyrin dianion; TPP, *meso*-tetraphenylporphyrin dianion; TPPS, *p*-tetrasulphophenylporphyrin dianion; TTP, *meso*-tetra-*p*-tolylporphyrin dianion; T(^{i}Pr$_3$P)P, *meso*-tetrakis(2,4,6-triisopropylphenyl)-porphyrin; TRP(R = Me, Et, ^{i}Pr, ^{c}Pr, or ^{n}Pr), dianion of meso-tetraalkylporphyrin where R is methyl (Me), ethyl (Et), isopropyl (^{i}Pr), cyclopropyl (^{c}Pr), or propyl (^{n}Pr); *p*-X-TPP, *meso*-tetrakis(*p*-substituted phenyl)-porphyrin dianion; 18-C-6, 1,4,7,10,13,16-hexaoxacyclooctadecane; PPN, bis(triphenylphosphine)nitrogen; N$_p$, porphyrinato nitrogen; THF, tetrahydrofuran; Py, pyridine; HIm, imidazole; 1-MeIm, 1-methylimidazole; 2-MeHIm, 2-methylimidazole; Kryptofix-222 or 222, 4,7,13,16,21,24-hexaoxo-1,10-diazabicyclo[8.8.8]hexacosane; TMPA, tris(2-pyridylmethyl)amine; NPy$_3$, tris(4-(pyridin-4-yl)phenyl)amine; Me$_6$tren, 2,2′,2″-tris(dimethy1amino)ethyl)amine.
(18) Armarego, W. L. F.; Perrin, D. D. *Purification of Laboratory Chemicals*; Butterworth-Heinemann: Oxford, England, 1997; p 413.
(19) Adler, A. D.; Longo, F. R.; Finarelli, J. D.; Goldmacher, J.; Assour, J.; Korsakoff, L. *J. Org. Chem.* **1967**, *32*, 476.
(20) Wagner, R. W.; Lawrence, D. S.; Lindsey, J. S. *Tetrahedron Lett.* **1987**, *28*, 3069;Lindsey, J. S.; Wagner, R. W. *J. Org. Chem.* **1988**, *54*, 828.
(21) (a) Adler, A. D.; Longo, F. R.; Kampus, F.; Kim, J. *J. Inorg. Nucl. Chem.* **1970**, *32*, 2443. (b) Buchler, J. W. In *Porphyrins and Metalloporphyrins*; Smith, K. M., Ed.; Elsevier Scientific Publishing: Amsterdam, The Netherlands, 1975; Chapter 5.
(22) Landergren, M.; Baltzer, L. *Inorg. Chem.* **1990**, *29*, 556.
(23) (a) Fleischer, E. B.; Srivastava, T. S. *J. Am. Chem. Soc.* **1969**, *91*, 2403;(b) Hoffman, A. B.; Collins, D. M.; Day, V. W.; Fleischer, E. B.; Srivastava, T. S.; Hoard, J. L. *J. Am. Chem. Soc.* **1972**, *94*, 3620.
(24) Scheidt, W. R.; Cohen, I. A.; Kastner, M. E. *Biochemistry* **1979**, *18*, 3546.
(25) Sheldrick, G. M. *Acta Crystallogr.* **1990**, *A46*, 467.
(26) Sheldrick, G. M. *Program for the Refinement of Crystal Structures*; Universität Göttingen,: Germany, 1997.
(27) $R_1 = \sum||F_o| - |F_c||/\sum|F_o|$ and $wR_2 = \{\sum[w(F_o^2 - F_c^2)^2]/\sum[wF_o^4]\}^{1/2}$. The conventional *R*-factors R_1 are based on *F*, with *F* set to zero for negative F^2. The criterion of $F^2 > 2\sigma(F^2)$ was used only for calculating R_1. *R*-factors based on F^2 (wR_2) are statistically about twice as large as those based on *F*, and *R*-factors based on ALL data will be even larger.
(28) Sheldrick, G. M. *Program for Empirical Absorption Correction of Area Detector Data*; Universität Göttingen: Germany, 1996.
(29) Macrae, C. F.; Bruno, I. J.; Chisholm, J. A.; Edgington, P. R.; McCabe, P.; Pidcock, E.; Rodriguez-Monge, L.; Taylor, R.; Streek, J.; van de Wood, P. A. *J. Appl. Crystallogr.* **2008**, *41*, 466;Macrae, C. F.; Edgington, P. R.; McCabe, P.; Pidcock, E.; Shields, G. P.; Taylor, R.; Towler, M.; van de Streek, J. *J. Appl. Crystallogr.* **2006**, *39*, 453;Bruno, I. J.; Cole, J. C.; Edgington, P. R.; Kessler, M. K.; Macrae, C. F.; McCabe, P.; Pearson, J.; Taylor, R. *Acta Crystallogr.* **2002**, *B58*, 389;Taylor, R.; Macrae, C. F. *Acta Crystallogr.* **2001**, *B57*, 815.
(30) Bondi, A. *J. Phys. Chem.* **1964**, *68*, 441.
(31) Scheidt, W. R. Coordination Chemistry and Materials. In *Handbook of Porphyrin Science*; Kadish, K. M., Smith, K., Guilard, R., Eds.; World Scientific: Singapore and Hackensack, NJ, 2012; Vol. *24*, pp 1−180.
(32) Rhynard, D.; Lang, G.; Spartalian, K.; Yonetani, T. *J. Chem. Phys.* **1979**, *71*, 3715.
(33) Silver, J.; Taies, J. A. *Inorg. Chim. Acta* **1989**, *159*, 231.
(34) Lukas, B.; Silver, J. *Inorg. Chim. Acta* **1986**, *124*, 97.
(35) Lukas, B.; Peterson, J.; Silver, J.; Wilson, M. T. *Inorg. Chim. Acta* **1983**, *80*, 245.
(36) Inniss, D.; Soltis, M.; Strouse, C. E. *J. Am. Chem. Soc.* **1988**, *110*, 5644.
(37) Ikeue, T.; Ohgo, Y.; Saitoh, T.; Yamaguchi, T.; Nakamura, M. *Inorg. Chem.* **2001**, *40*, 3423.
(38) Walker, F. A. In *The Porphyrin Handbook*; Kadish, K. M., Smith, K. M., Guilard, R., Eds.; Academic Press: New York, 2000; Vol. *5*, p 132.
(39) Wojaczynski, J.; Latos-Grazynski, L.; Glowiak, T. *Inorg. Chem.* **1997**, *36*, 6299.
(40) Scheidt, W. R.; Lee, Y. J.; Luangdilok, W.; Haller, K. J.; Anzai, K.; Hatano, K. *Inorg. Chem.* **1983**, *22*, 1516.
(41) Scheidt, W. R.; Haller, K. J.; Hatano, K. *J. Am. Chem. Soc.* **1980**, *102*, 3017.
(42) Scheidt, W. R.; Hatano, K. *Acta Chrystallogr.* **1991**, *C47*, 2201.
(43) Bartczak, T. J.; Wolowiee, S.; Latos-Grazynski, L. *Inorg. Chim. Acta* **1998**, *277*, 242.
(44) Schappacher, M.; Fischer, J.; Weiss, R. *Inorg. Chem.* **1989**, *28*, 389.
(45) Balch, A. L.; Noll, B. C.; Safari, N. *Inorg. Chem.* **1993**, *32*, 2901.
(46) Corsi, D. M.; Murthy, N. N.; Young, V. G., Jr.; Karlin, K. D. *Inorg. Chem.* **1999**, *38*, 848.
(47) Scott, M. J.; Lee, S. C.; Holm, R. H. *Inorg. Chem.* **1994**, *33*, 4651.
(48) Walker, F. A.; Nasri, H.; Turowska-Tyrk, H.; Mohanrao, K.; Watson, C. T.; Shokhirev, N. V.; Debrunner, P. G.; Scheidt, W. R. *J. Am. Chem. Soc.* **1996**, *118*, 12109.
(49) Simonneaux, G.; Schunemann, V.; Morice, C.; Carel, L.; Toupet, L.; Winkler, H.; Trautwein, A. X.; Walker, F. A. *J. Am. Chem. Soc.* **2000**, *122*, 4366.
(50) Yatsunyk, L. A.; Walker, F. A. *Inorg. Chem.* **2004**, *43*, 4341.
(51) Scheidt, W. R.; Reed, C. A. *Chem. Rev.* **1981**, *81*, 543.
(52) Hoard, J. L. *Ann. N. Y. Acad. Sci.* **1973**, *206*, 18.
(53) Pombeiro, A. J. L.; Fatima, M.; Silva, C. G. D. *J. Organomet. Chem.* **2001**, *617*, 65.
(54) Lee, S. C.; Scott, M. J.; Kauffmann, K.; Munck, E.; Holm, R. H. *J. Am. Chem. Soc.* **1994**, *116*, 401.
(55) Dalosto, S. D.; Vanderkooi, J. M.; Sharp, K. A. *J. Phys. Chem. B* **2004**, *108*, 6450.
(56) Milani, M.; Ouellet, Y.; Ouellet, H.; Guertin, M.; Boffi, A.; Antonini, G.; Bocedi, A.; Mattu, M.; Bolognesi, M.; Ascenzi, P. *Biochemistry* **2004**, *43*, 5213.
(57) Yoshikawa, S.; O'Keeffe, D. H.; Caughey, W. S. *J. Biol. Chem.* **1985**, *260*, 3518.
(58) Reddy, K. S.; Yonetani, T.; Tsuneshige, A.; Chance, B.; Kushkuley, B.; Stavrov, S. S.; Vanderkooi, J. M. *Biochemistry* **1996**, *35*, 5562.
(59) Fukuyama, K.; Kunishima, N.; Amada, F.; Kubota, T.; Matsubara, H. *J. Biol. Chem.* **1995**, *270*, 21884.
(60) Debrunner, P. In *Iron Porphyrins Part 3*; Lever, A. B. P., Gray, H. B., Eds.; VCH Publishers Inc.: New York, 1983; Chapter 2.
(61) Walker, F. A.; Huynh, B. H.; Scheidt, W. R.; Osvath, S. R. *J. Am. Chem. Soc.* **1986**, *108*, 5288.
(62) Scheidt, W. R.; Kirner, J. F.; Hoard, J. L.; Reed, Ch. A. *J. Am. Chem. Soc.* **1987**, *109*, 1963.
(63) Walker, F. A. *Coord. Chem. Rev.* **1999**, *185*, 471.
(64) Migita, C. T.; Iwaizumin, M. *J. Am. Chem. Soc.* **1981**, *103*, 4378.
(65) Tsai, A.; Palmer, G. *Biochim. Biophys. Acta* **1982**, *681*, 484.

DOI: 10.1021/acs.inorgchem.5b00780
Inorg. Chem. 2015, 54, 6472−6485

(66) Yatsunyk, L. A.; Carducci, M. D.; Walker, F. A. *J. Am. Chem. Soc.* **2003**, *125*, 15986.
(67) Yatsunyk, L. A.; Dawson, A.; Carducci, M. D.; Nichol, S.; Walker, F. A. *Inorg. Chem.* **2006**, *45*, 5417.
(68) Orme-Johnson, N. R.; Hansen, R. E.; Beinert, H. *Biochem. Biophys. Res. Commun.* **1971**, *45*, 871.
(69) Salerno, J. C. J. *Biol. Chem.* **1984**, *259*, 2331.
(70) Safo, M. K.; Walker, F. A.; Raitsimring, A. M.; Walters, W. P.; Dolata, D. P.; Debrunner, P. G.; Scheidt, W. R. *J. Am. Chem. Soc.* **1994**, *116*, 7760.

DOI: 10.1021/acs.inorgchem.5b00780
Inorg. Chem. 2015, 54, 6472−6485